Ring-Strain-Modified Properties of Substituted Perylene Radical-Cation Salts. A Solid-State ^{13}C CPMAS NMR Study

P. Michel,[1a,b] A. Moradpour,*[,1a] P. Penven,[1a,b] L. Firlej,[1c,d] P. Bernier,[1c] B. Levy,[1e] S. Ravy,[1a] and A. Zahab[1c]

Contribution from the Laboratoire de Physique des Solides, Bâtiment 510, and Groupe de Chimie Quantique (LPCR), Bâtiment 337 (UA 2 and UA 75 of CNRS), Université de Paris-Sud, 91405 Orsay, France, Thomson-Sintra-ASM, Route de Ste. Anne du Portzic, 29601 Brest, France, and Groupe de Dynamique des Phases Condensées (UA 233) USTL, Place Eugène Bataillon, 34060 Montpellier, France. *Received March 6, 1990*

Abstract: We have considered the stereochemical distorsions of the molecular building blocks as a way to control the structure to properties relationships of organic conductive solids. 1,2,7,8-Tetrahydrodicyclopenta[*cd,lm*]perylene (CPP) and 3,4,9,10-tetramethylperylene (TMP), bearing sterically hindered substituents that involve strain-induced distorsions of the perylene skeleton, have been synthesized. Two conductive radical-cation salts, $CPP_2PF_6{\cdot}CH_2Cl_2$ and $TMP_2PF_6{\cdot}CH_2Cl_2$, have been prepared from these two strained donors by galvanostatic electrocrystallizations at −20 °C in CH_2Cl_2. These two salts are isostructural (monoclinic, space group $C_{2/m}$). The structures consist of similar regular stacks of the almost planar donors (the bond lengths and angle values being distorted as expected) along the crystallographic *c* axis. The refinements of the structures (final $R = 0.0946$ for CPP and $R = 0.1365$ for the TMP salt) have been difficult because of the disorder of the counterions and of the solvent contained in the channels between the organic stacks. Solid-state ^{13}C CPMAS NMR, has been used to study both salts. They exhibit two different locally resolved ^{13}C conduction electron Knight shift sets. The calculated values of the spin density distributions and the derived electron–nuclear hyperfine coupling constants allow an almost complete and unambiguous assignment of the Knight shifts, as well as the graphical estimation of the unknown Pauli magnetic susceptibilities. These observed modifications of the Knight shift patterns, when these salts are compared to each other, are related to the molecular strain-induced distorsions and they reflect significant changes in the local electronic structures. This supports the possibility of using stereochemical factors as a new way to monitor the bulk physical behavior of organic metals.

Introduction

The electronic delocalization throughout organic conducting solids results from intermolecular π electron overlaps along quasi one-dimensional (1-D) stacks of planar unsaturated open-shell organic molecules. The physical properties of these solids are due to the existence of the delocalized conduction electrons and depend primarily on the chemical nature of the building blocks, as well as on the interactions of the latter within the solid lattices. Thus, for example, superconductivity is almost exclusively observed with tetramethyltetraselenafulvalene (TMTSF)[2] and bis(ethylenedithio)tetrathiofulvalene (BEDT-TTF).[3] This remarkable physical property[4] is then determined within each family of the (1-D) radical-cation salts $TMTSF_2X$ ($X = PF_6^-$, ClO_4^-) and $(BEDT\text{-}TTF)_2X$ ($X = I_3^-$, $CuSCN^-$) by (i) the intrastack packing factors determining the π-orbital overlap efficiencies along the stacking direction (ion size effects[5,6]) and (ii) the interstack intermolecular proximity interactions defining nonnegligible electronic diffusive motions in directions other than the main delocalization path (dimensionality effects[5,6]). In fact, both of these solid-state-mediated overlap interactions depend, at first, *on the molecular orbital characteristics of the building units*. The orbital patterns depend, on the other hand, on the stereochemistry of the latter. Consequently, modifications of the stereochemistry of the molecular components might be an interesting additional way to control the structure to properties relationships, within a series of (1-D) organic conducting materials.

Chart I

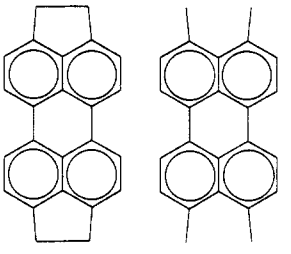

CPP 1 TMP 2

The stereochemical criteria have been very seldom considered for organic metals because the unsaturated heterocycles used to elaborate these solids have generally almost planar structures, and few studies have been published in this area: a conformationally driven solid-state structural modification, in the BEDT-TTF series, has been nicely correlated with the physical behavior of the so-called β^* $(BEDT\text{-}TTF)_2I_3$ phase;[7] a very interesting chiral substrate for organic conductors has been described[8,9] and low-dimensional conducting salts from a highly out-of-plane distorted polyarene have also been recently obtained.[10]

(1) (a) Laboratoire de Physique des Solides, Université de Paris-Sud. (b) Thomson-Sintra-ASM. (c) Groupe de Dynamique des Phases Condensées. (d) On leave from Institut of Molecular Physics, Polish Academy of Science, 60-179 Poznan, Poland. (e) Groupe de Chimie Quantique (LPCR), Université de Paris-Sud.

(2) (a) Proceedings of the International Conference on the Physics and the Chemistry of Synthetic and Organic Metals, Les Arcs, France. In *J. Phys., Colloq.* **1983**, *C3*, 44. (b) Proceedings of the International Conference on the Physics and Chemistry of Low Dimensional Synthetic Metals, AbanoTerme, Italy. In *Mol. Cryst. Liq. Cryst.* **1985**, 117–121.

(3) (a) Proceedings of the International Conference on Science and Technology of Synthetic Metals, Kyoto, Japan. In *Synth. Met.* **1987**, 17–19. (b) Proceedings of the International Conference on Science and Technology of Synthetic Metals, Santa Fe, NM, In *Synth. Met.* **1989**, 27–29.

(4) High conductivities have been obtained in complexes prepared from 4,5-dimercapto-1,3-dithiol-2-thione (H_2dmit); see: Bousseau, M.; Valade, L.; Legros, J. P.; Cassoux, P.; Garbanskas, M.; Interrante, L. V. *J. Am. Chem. Soc.* **1986**, *108*, 1908. Superconductivity has also been observed in this family for $TTF[Ni(dmit)_2]_2$: Brossard, M.; Ribault, M.; Bousseau, M.; Valade, L.; Cassoux, P. *C.R. Acad. Sci., Paris, Ser. 2* **1986**, 302, 205. For $[(CH_3)_4N][Ni(dmit)_2]_2$: Kobayashi, A.; Kim, H.; Sasaki, Y.; Kato, R.; Kobayashi, H.; Moriyama, S.; Nishio, Y.; Kajita, K.; Sasaki, W. *Chem. Lett.* **1987**, 1819.

(5) Wudl, F. *Acc. Chem. Res.* **1984**, *17*, 227, and references cited therein.

(6) Williams, J. M.; Beno, M. A.; Wang, H. H.; Leung, P. C. W.; Emge, T. J.; Geiser, U.; Carlson, K. D. *Acc. Chem. Res.* **1985**, *18*, 261, and references cited therein.

(7) Schultz, A. J.; Wang, H. H.; Williams, J. M. *J. Am. Chem. Soc.* **1986**, *108*, 7853.

(8) Wallis, J. D.; Karrer, A.; Dunitz, J. D. *Helv. Chim. Acta* **1986**, *69*, 69.

(9) Freund, M. M.; Olsen, J. L.; Wallis, J. D.; Karrer, A.; Dunitz, J. D.; Hilti, B. *Jpn. J. Appl. Phys., Part 1* **1987**, *26* (Suppl. 26–3), 895.

(10) Michel, P.; Moradpour, A.; Ribault, M.; Petit, P.; André, J. J. *J. Chem. Soc., Chem. Commun.* **1989**, 1173.

0002-7863/90/1512-8285$02.50/0

Thus, it seems attractive to examine the influence of molecular stereochemical distortions [resulting in electronic (spin and charge) modifications] of the parent donors on the solid-state properties of the resulting conducting salts. A possibility to monitor such distortions is given by the modifications of the strain, exhibited by aromatic rings, as a consequence of the introduction of various sterically hindered substituents. We decided to synthesize appropriately substituted polyaromatic compounds and to investigate the solid radical-cation salts obtained from these strained donors.

We have prepared two substituted perylenes: 1,2,7,8-tetrahydrodicyclopenta[*cd*,*lm*]perylene (CPP, **1**)[11] and 3,4,9,10-tetramethylperylene (TMP, **2**).[12]

In this series, in addition to the salts from perylene itself,[13] a report of a study on a salt prepared from **1** was published some time ago.[14] However, the stereochemical strain-mediated aspects of this donor had not been considered in this study. We have now produced a parent cation-radical salt from **2** and have found these two salts to be isostructural. We report here the results of a comparative study of the latter by high-resolution solid-state ^{13}C CPMAS NMR spectroscopy.[15]

NMR of solids,[16] as a rapidly expanding technique, has been applied, until now, to few organic molecular conductors.[17]

In this area, this method offers the unique possibility to focus on the magnetic behavior of every single atomic site involved in cooperative solid-state conduction phenomena. This possibility is derived from the Knight shifts, which originate from the polarization, by the external magnetic field, of the conduction electron-gas interacting with the nuclei. These shifts are very sensitive to the molecular electron spin distributions within the conducting solids; therefore, a detailed insight is possible into the local electronic properties of an organic metal.

The present study is the first example of the implication, in the solid-state behavior of conducting solids, of the electron spin distributions mediated by ring-strain distorsions of the molecular components. This stereochemical control of the solid-state properties is outlined by ^{13}C CPMAS NMR, which appears to be a unique local probe to investigate the electronic properties of these solids, on both the molecular and the solid-state levels.

Experimental Section

Syntheses, Electrochemical Instrumentation, and UV–vis Spectra. 1,2,7,8-Tetrahydrocyclopenta[*cd*,*lm*]perylene (**1**, CPP) was synthesized according to the literature procedure,[11] and 3,4,9,10-tetramethylperylene (**2**, TMP) was prepared as previously described.[12] Cyclic voltammetry was carried out on a EG & G PAR 273 potentiostat and a Sefram TGM 164 X–Y recorder. Electronic absorption spectra were recorded with a Varian Cary 219 instrument. **1**: (ethanol) λ_{max}, nm (ϵ) 455 (41 000), 426.5 (29 000), 403 (12 800), 260.5 (23 000), 254 (21 000), 249 (20 000). **2**: (ethanol) 453 (8400), 427 (7350), 405 (4400) (sh), 262.5 (12 700), 255 (11 800).

Preparation of the Radical-Cation Salts by Electrocrystallization. Solutions of **1** or **2** (1.5×10^{-3} mol·dm^{-3}) in dry CH_2Cl_2, containing 1.5×10^{-2} mol·dm^{-3} tetrabutylammonium hexafluorophosphate, were galvanostatically electrocrystallized at −20 °C (current densities ~0.3 μA·cm^{-2} on platinum electrodes); electrocrystallizations were stopped after a time corresponding to approximately 30% of the calculated Faradaic equivalent required for a total oxidation of the donor. The black shiny monocrystalline needles, grown in the anodic compartment, were collected by filtration and washed with a small amount of dry CH_2Cl_2. Anal. Calcd for $(CPP)_2PF_6 \cdot CH_2Cl_2$, $C_{49}H_{34}Cl_2F_6P$ (838.19): C, 70.15; H, 4.09; Cl, 8.46. Found: C, 69.72; H, 4.20; Cl, 8.21. Anal. Calcd for $(TMP)_2PF_6$, CH_2Cl_2, $C_{49}H_{42}Cl_2F_6P$ (846.25): C, 69.48; H, 5.00; Cl, 8.38. Found: C, 69.55; H, 4.95; Cl, 8.41.

Molecular and Crystal Structure Determinations. The X-ray diffraction data were collected by using an Enraf-Nonius four-circle diffractometer with the Mo Kα (λ = 0.710 69 Å) monochromatized radiation; the structures[18] were solved by an SDP program. The diffuse-scattering experiments were performed by the fixed-film fixed-crystal method,[19] using a Cu Kα monochromatized beam.

Extended Hückel MO, Spin Densities, and Molecular Mechanics Calculations. Calculations were performed with the HP(9000-825) computer of the Groupe de Chimie Quantique; extended Hückel calculations (EHC) were done with a program[20] kindly supplied by E. Amouyal and G. Calzaferri; π spin densities have been calculated by the Hoijtinck method[21] with the following modifications: the unperturbed Hamiltonian H_0 has been chosen as the sum over $(2n - 1)$ electrons of the one-electron Fock operator $F(\nu)$, constructed with the MOs calculated for the neutral molecule.

$$H_0 = \sum_{\nu=1}^{2n-1} F(\nu)$$

The present choice is not the most usual one, which assumes that this operator is constructed with the MOs of the radical itself;[21] however, it is consistent with the fact that MOs and the orbital energies have been obtained by an EHC of the neutral molecules (using the geometries of the radicals). Consequently, the matrix elements in the perturbation formulas are modified:

$$\langle\psi_0|2S_zD_i|\phi_k\rangle = \langle\varphi_k|D_i|\pi_n\rangle$$

$$\langle\psi_0|2S_zD_i|\phi_l\rangle = \langle\pi_n|D_i|\varphi_l\rangle$$

$$\langle\psi_0|2S_zD_i|\phi_{kl,1}\rangle = 0$$

$$\langle\psi_0|2S_zD_i|\phi_{kl,2}\rangle = \sqrt{2/3}\langle\varphi_k|D_i|\varphi_l\rangle$$

$$\langle\psi_0|\mathcal{V}|\phi_k\rangle = 0$$

$$\langle\psi_0|\mathcal{V}|\phi_l\rangle = -\langle\pi_n|J_n|\varphi_l\rangle$$

$$\langle\psi_0|\mathcal{V}|\phi_{kl,1}\rangle = (1/\sqrt{2})\langle\varphi_k|2J_n - K_n|\varphi_l\rangle$$

$$\langle\psi_0|\mathcal{V}|\phi_{kl,2}\rangle = -\sqrt{3/2}\langle\varphi_k|K_n|\varphi_l\rangle$$

The zeroth-order wave function ψ_0 is

$$\psi_0 = |\ldots \varphi_k\overline{\varphi_k} \ldots \pi_n|$$

The excited states Φ_k have been defined as

$$\Phi_k = |\ldots \varphi_k \ldots \pi_n\overline{\pi_n}|$$

$$\Phi_l = |\ldots \varphi_k\overline{\varphi_k} \ldots \varphi_l|$$

$$\phi_{kl,1} = (\phi_{kl,A} - \phi_{kl,C})/\sqrt{2}$$

$$\phi_{kl,2} = (\phi_{kl,A} - 2\phi_{kl,B} + \phi_{kl,C})\sqrt{6}$$

$$\Phi_{kl,A} = |\ldots \varphi_k \ldots \pi_n\varphi_l|$$

$$\Phi_{kl,B} = |\ldots \varphi_k \ldots \pi_n\psi_l|$$

$$\Phi_{kl,C} = |\ldots \varphi_k \ldots \pi_n\varphi_l|$$

where φ_k is a doubly occupied orbital in the zeroth-order wave function

(11) Tanaka, N.; Kasai, T. *Bull. Chem. Soc. Jpn.* **1981**, *54*, 3026.
(12) Michel, P.; Moradpour, A. *Synthesis* **1988**, 894.
(13) Keller, H. J.; Nöthe, D.; Pritzkow, H.; Wehe, D.; Werner, M.; Koch, P.; Schweitzer, D. *Mol. Cryst. Liq. Cryst.* **1980**, *62*, 181.
(14) Lapouyade, R.; Morand, J. P.; Chasseau, D.; Hauw, C.; Delhaes, P. In: Reference 2a, p 1235.
(15) A preliminary report on a part of these results has been communicated: Firlej, L.; Bernier, P.; Zahab, A.; Michel, P.; Moradpour, A.; Penven, P.; Levy, B. Annual Meeting of the American Physical Society, Anaheim, CA, March 1990.
(16) (a) Maciel, G. E. *Science* **1984**, 226, 282, and references cited therein. (b) Fife, C. A.; *Solid State NMR for Chemists*; CRS Press: Guelph, 1983. (c) Chmelka, B. F.; Pines, A. *Science* **1989**, *246*, 71.
(17) (a) Rybaczewski, E. F.; Smith, L. S.; Garito, A. F.; Heeger, A. J.; Silbernagel, B. G. *Phys. Rev. B.* **1976**, *14*, 2746. (b) Mehring, M.; Spengler, J. *Phys. Rev. Lett.* **1984**, *53*, 2441. (c) Bernier, P.; Audenaert, M.; Schweizer, R. J.; Stein, P. C.; Jérome, D.; Bechgaard, K.; Moradpour, A. *J. Phys. Lett.* **1985**, *46*, L-675. (d) Stöcklein, W.; Seidel, H. H.; Singel, D.; Kendrick, R. D.; Yannoni, C. S. *Chem. Phys. Lett.* **1987**, *141*, 277. (e) Wieland, J.; Haeberlen, U.; Schweitzer, D.; Keller, H. J. *Synth. Met.* **1987**, *19*, 393. (f) Stein, P. C.; Bernier, P.; Lenoir, C. *Phys. Rev. B.* **1987**, *35*, 4389. (g) Toscano, P. J.; Marks, T. J. *J. Am. Chem. Soc.* **1986**, *108*, 437.
(18) More complete crystallographic details will be published in the future: Penven, P.; Batail, P., to be published.
(19) Comès, R.; Shirane, G. In *Highly Conducting One-Dimensional Solids*; Devreese, J. T.; Evrard, R. P.; Van Doren, V.-E., Eds.; Plenum Press: New York, 1979.
(20) Calzaferri, G.; Forss, L. *QCPE* **1974**, *No. 344*. See also: Calzaferri, G.; Forss, L.; Kamser, I. *J. Phys. Chem.* **1989**, *93*, 5366.
(21) Hoijtink, G. J. *Mol. Phys.* **1958**, *1*, 158.

Scheme I

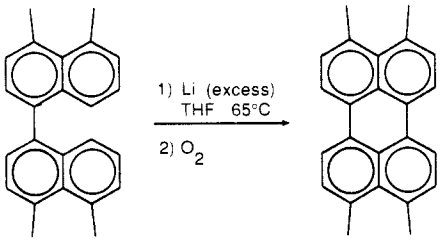

3 **2**

ψ_0. π_n the singly occupied orbital, and φ_l a virtual orbital, and the evaluation of the matrix elements of D_l is straightforward (see the text, eq 3). Concerning J_n and K_n (J_n and K_n are the Coulomb and exchange operators corresponding to the unpaired orbital π_n of ψ_0), we have expressed them in terms of integrals over the AOs, retaining only the two center contributions (pp, qq) (zero differential overlap approximation):

$$(pp, qq) = \int |\chi_p(r_1)|^2 |\chi_q(r_2)|^2 / r_{12}\, dr_1\, dr_2$$

where r_1 and r_2 are the vector positions of the two electrons 1 and 2 and $r_{12} = |r_1 - r_2|$. There are explicit formulas for these integrals (pp, qq) when χ_p and χ_q are standard $2p_\pi$ orbitals.[22] One just needs to define the geometry of the system and the exponents ζ of the exponential factor of the orbitals; we have used here the same geometry and the same ζ (ζ = 1.625) as the ones used for evaluating the overlaps in EHC.

Finally, the π spin densities of the methyl and methylene substituants have been obtained by a hyperconjugation-type calculation. It turns out that, in this way, some small π spin density values are also found for the fictitious π orbitals f_H, standing for the out-of-plane H atoms, (ρ_{f_H} = +0.0172 for CPP and ρ_{f_H} = +0.0131 for TMP); the contribution of these densities to the derived hyperfine coupling constants is not significant (see Table VII).

The strain energy content of the two donors was determined by Allinger-type (MMX) molecular mechanics calculations; a PC MODEL version of C. Still's MODEL program (Serena Software) was used. E. Noizet (Laboratoire des Mécanismes Réactionnels, Ecole Polytechnique) is gratefully acknowledged for these calculations.

^{13}C CPMAS NMR Measurements. NMR spectra were recorded on powdered samples with a Brücker CXP spectrometer, working at 50.3 MHz. Magic angle spinning (MAS) at frequencies larger than 2 kHz, cross polarization (CP), and proton decouplings were used to obtain high resolutions and sensitivities. The cross-polarization contact time was optimized by analyzing the signal intensity variations and the value of 2 ms was employed; the repetition time for all spectra was fixed to 3 s. About 2000 scans were required to obtain satisfactory spectra with all studied samples (~50 mg of the solids). The usual gated decoupling (dipolar-dephasing) technique[16] was used to differentiate carbons bonded to (or in the vicinity of) protons. The chemical shifts were measured by reference to TMS via adamantane as a secondary reference.

Results

(a) Syntheses of the Donors and Determination of the Strain Energies and the Electrochemical Properties. We have synthesized TMP **2** starting from the easily available 4,4',5,5'-tetramethyl-1,1'-dinaphthalene (**3**);[12] a significant difference appeared at this very first stage of our study for the synthesis of the substituted perylenes **1** and **2**: although this easy one-step Li-mediated cyclodehydrogenation leads to **2** with an acceptable 40% yield (Scheme I), this reaction had not been successful for the isolation of **1**. The latter was prepared, as described previously, from 5,6-dilithioacenaphthalene by a Co(II)-medicated coupling reaction.[11] The isolated compound **1** was subsequently found to be unstable in the highly reducing media needed for the lithium-mediated synthesis of **2**.

The strain energy, as compared to perylene, was determined by MMX calculations and found to be higher for **1** (18.7 kcal·mol^{-1}) than **2** (15.9 kcal·mol^{-1}).

The redox potentials (Table I) of these two donors **1** and **2** reveal also marked differences as compared to the unsubstituted parent compound. First, the substitutions lead to a predictable lowering of the oxidation potentials compared to perylene, but a surprisingly high difference (180 mV) between the oxidation potentials is measured for **1** and **2**. These results also reflect, in the reduction part of the scanned potentials, the dramatic unstability of **1**, already noticed during the syntheses; in fact, whereas reduction waves are observed both for perylene and **2**, no such wave is observable by cyclic voltammetry with **1** using scan rates up to 1 V·s^{-1}.

Table I. Electrochemical Results

compound[a]	$E^a_{p/2}$,[b,c] V	$E^c_{p/2}$,[b,c] V
perylene	+1.03	−1.85
CPP (**1**)	+0.62	*d*
TMP (**2**)	+0.80	−1.79

[a] All compounds are approximately 1 mM in CH_2Cl_2 for oxidation waves, or THF for reductions, with 0.1 M tetrabutylammonium hexafluorophosphate. [b] Potentials vs SCE of the first waves. [c] Scan rates of 100 mV·s^{-1}. [d] No reduction wave detected up to 1 V·s^{-1}.

Table II. Crystal Data

	$(CPP)_2PF_6{\cdot}CH_2Cl_2$	$(TMP)_2PF_6{\cdot}CH_2Cl_2$
formula	$C_{48}H_{32}PF_6{\cdot}CH_2Cl_2$	$C_{48}H_{40}PF_6{\cdot}CH_2Cl_2$
mol wt	838.18	846.25
crystal system	monoclinic	monoclinic
space group	$C_{2/m}$	$C_{2/m}$
Z[a]	1	1
a, Å	16.262 (3)	15.814 (2)
b, Å	12.627 (2)	13.684 (3)
c, Å[a]	4.433 (2)	4.463 (4)
β, deg	100.90 (3)	101.30 (2)
V, Å^3	892.6	948.4
d_{calcd}, g/cm^3	1.600	1.472
no. of reflctns collected	661	704
no. of reflctns used ($I > 3\sigma(I)$)	487	429
R	0.0946	0.1365
R_w	0.1418	0.1872

[a] The reported structure refinements have been obtained by neglecting the anion and solvent positions and this accounts for Z = 1. The actual value is Z = 2 (c = 8.866 Å) corresponding to the 2:1:1 stoichiometry.

(b) Preparation of the Cation-Radical Salts and Crystal and Molecular Structure Parameters. The polyarene family of organic metals,[23] which exhibits very interesting properties,[24] has been studied (with very few exceptions) starting with the only commercially available polyaromatic compounds.[25] The radical-cation salts of the latter (such as pyrene, perylene, azulene) were prepared by electrocrystallization[26] long before the discovery of the first organic superconductor,[27] which gave this technique its present wide use as the way to prepare conducting organic solids.

Both donors CPP and TMP easily form nice shiny black monocrystals of the 2:1 salts grown by this electrocrystallization process.

The dc electrical conductivity of these radical-cation salts has been measured by the four-probe method along the needle axis. The values of the resistivity σ at 295 K are found to be

$$(CPP)_2PF_6{\cdot}CH_2Cl_2: \quad \sigma = 50\ \Omega^{-1}{\cdot}cm^{-1}$$ [14]

$$(TMP)_2PF_6{\cdot}CH_2Cl_2: \quad \sigma = 5\ \Omega^{-1}{\cdot}cm^{-1}$$

A similar smooth transition, for both conducting salts, to a semiconducting state—already noticed for $(CPP)_2PF_6{\cdot}CH_2Cl_2$[14]—is observed just below room temperature.[28]

(22) Roothaan, C. C. J. *J. Chem. Phys.* **1951**, *19*, 1445.

(23) Kröhnke, C.; Enkelmann, V.; Wegner, G. *Angew. Chem., Int. Ed. Engl.* **1980**, *19*, 912.

(24) See, for example: Dormann, E.; Sachs, G.; Stocklein, W.; Bail, B.; Schwoerer, M. *Appl. Phys.* **1983**, *A30*, 227.

(25) Enkelmann, V. In: Reference 2a, p 1147, and references cited therein.

(26) Chiang, T. C.; Reddoch, A. H.; Williams, D. F. *J. Chem. Phys.* **1971**, *54*, 2051.

(27) Jérome, D.; Mazaud, A.; Ribault, M.; Bechgaard, K. *J. Phys. Lett., Paris* **1980**, *41*, L-95.

(28) The detailed studies of the physical measurements for this series of radical cation salts will be published in a forthcoming paper: Penven, P.; Auban, P.; Jérome, D., to be published.

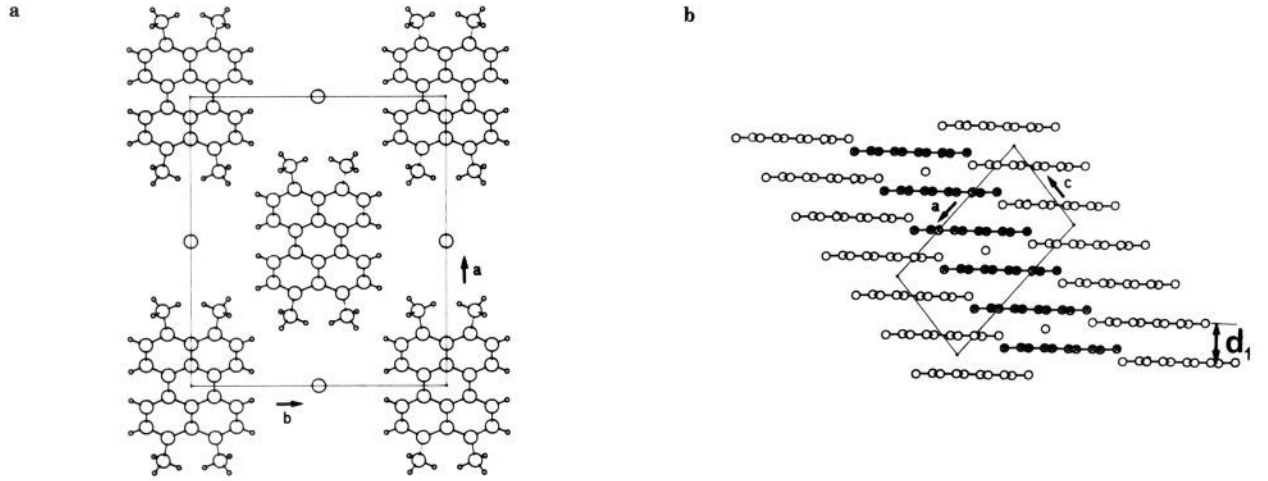

Figure 1. Crystal structure of $TMP_2PF_6{\cdot}CH_2Cl_2$ viewed along (a) the c axis and (b) along the b axis (for d_1, see the text).

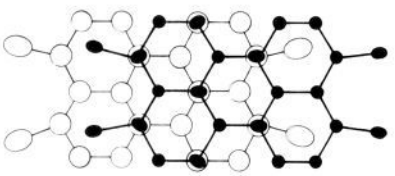

Figure 2. Molecular overlap schematized for both CPP and TMP salts.

In sharp contrast to various salts prepared from perylene itself by these anodic oxidations,[13] multiphasic salt formation is now suppressed. Single-phase formations are generally observed for a given solvent and temperature.[29]

(i) Crystal Structures. The crystal data are summarized in Table II. Almost identical unit cell parameters as well as very similar, regular, isolated stacks of the almost planar donor are found for both salts. The unit cell views for $(TMP)_2PF_6{\cdot}CH_2Cl_2$ along the c axis and the b axis are shown in Figure 1, parts a and b, respectively (CH_2Cl_2 and PF_6 anions are not shown). The intrastack overlap for both donors is schematized in the Figure 2.

The angles between the stacking axis (c axis) and the perpendicular to the mean planes of the donors are found to be identical (38.89° for TMP and 38.90° for CPP salt) for both solids; the distances d_1 (Figure 1b) between mean planes containing two consecutive molecules within a stack are also very close: d_1 = 3.474 Å (TMP) and 3.450 Å (CPP). However, if the anions and the solvent molecules located between the stacks are considered, the refinements of the structures were very difficult, due to a disorder of the former (see Table II, R and R_w values).

This problem was further investigated by X-ray diffuse scattering. This technique is based on the study of the scattering at angles different from the Bragg angles, which is due to some deviations from the perfect crystal periodicities.[19] The results obtained for the CPP- and TMP-based materials are shown in Figure 3.

In these experiments the c axis was almost vertical. These photographs reveal additional diffuse lines between the layer of Bragg spots $l = n$ (n integer). For both compounds, some reinforcements along the diffuse lines are also clearly visible. Although the diffuse lines seem as intense as the fundamental reflections because of the long exposure time, their intensity is actually 1 or 2 orders of magnitude lower than the latter. These lines give the true periodicity of the lattice in the stacking direction, which is in fact $2c$. For both solids, the width of these diffusions along c is the same as the Bragg spots, indicating long-range order in the c direction. Considering the stoichiometry of the salts (2:1:1), this long-range order involves the fillings of the channels between

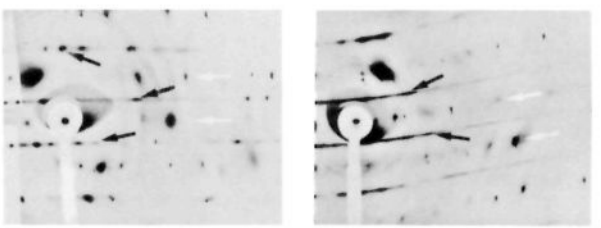

(a) (b)

Figure 3. X-ray patterns obtained for (a) $CPP_2PF_6{\cdot}CH_2Cl_2$ and (b) $TMP_2PF_6{\cdot}CH_2Cl_2$. The c axis is nearly vertical in both cases; diffuse lines are found at half-distance between the layers of Bragg spots (white arrows). Along the diffuse lines, the reinforcements are pointed out by the black arrows. These reinforcements are found to be much wider for the TMP salt (b).

the organic stacks by regular alternations of PF_6 anions and CH_2Cl_2 molecules. However, differences between the two salts are found when the shapes of the diffuse lines are considered: the reinforcements along the diffuse lines are much wider for the TMP than for the CPP salt (Figure 3). This phenomenon indicates that the ordered lines (along the c axis) of the alternating PF_6^- and CH_2Cl_2 are more correlated within the (a, b) plane, for the CPP salt. Although a more elaborate analysis of this disorder is needed,[30] it appears clear now that (i) $(CPP)_2{\cdot}PF_6{\cdot}CH_2Cl_2$ is more ordered than $(TMP)_2PF_6{\cdot}CH_2Cl_2$ and (ii) the unit cells are doubled in the c direction (see footnote for Table II).

(ii) Molecular Structures. Besides the crystal structures, molecular bond length and angle values, for the almost planar CPP and TMP were determined within the stacks of both solid salts $(CPP)_2{\cdot}PF_6{\cdot}CH_2Cl_2$ and $(TMP)_2PF_6{\cdot}CH_2Cl_2$. Some selected values of bond lengths and angles are summarized in Figure 4.

As expected, the presence of the five-membered saturated rings in CPP (Figure 4a) and the nonbonded repulsive interactions between the methyl substituents in TMP (Figure 4b) results in considerable in-plane distortions of the molecular geometries. The modifications of the angle values from the ideal 120°, for these donors, might be compared with the corresponding modifications obtained in the naphthalene series with the same substituents, as measured for 1,8-dimethylnaphthalene[31] and acenaphthalene.[32] In the present case, the bond lengths are much more affected by the strain, probably because of the doubly substituted structures

(29) Other 5:3 or 4:3 stoichiometries were obtained if THF, for example, is used as a solvent at −20 °C; these salts are studied separately.

(30) The results of the detailed studies of diffuse scattering experiments on this series of conducting salts will be published in a forthcoming article (work in progress).

(31) Bright, D.; Maxwell, I. E.; De Boer, J. *J. Chem. Soc., Perkin Trans. 2* **1973**, 2101.

(32) Hazell, A. C.; Hazell, R. G.; Norskov-Lauristen, L.; Briant, C. E.; Jones, D. W. *Acta Crystallogr.* **1986**, *C42*, 690.

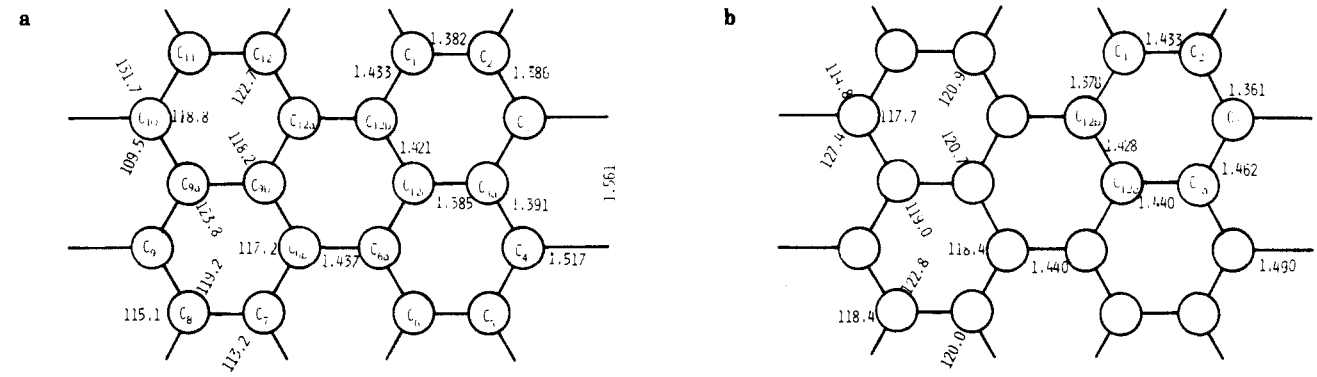

Figure 4. Principal bond lengths (Å) and angles (deg) of (a) $CPP_2PF_6 \cdot CH_2Cl_2$ and (b) $TMP_2PF_6 \cdot CH_2Cl_2$. For the atomic numbering scheme of perylene, see (a).

Table III. Chemical Shifts[a] of the Various Carbon Positions for the Neutral Donors in the Solid State

carbon position	CPP	TMP	carbon position	CPP	TMP
C(1)	121	121	C(12c)	127	131
C(2)	121	121	C(12b)	146	137
C(3)	140	135	$-(CH_2)_2-$ (or CH_3)	28	26
C(3a)	127	131			

[a] In ppm from Me_4Si.

of our substrates. Thus, the distance C(3)–C(3a) is shorter by more than 0.07 Å going from TMP to CPP (Figure 4), whereas bond distortions of, at most, 0.04 Å are found in the naphthalene series with the same substituents.[31,32]

(c) Extended Hückel MO Calculations. Taking into account the strain-induced molecular geometry distortions measured above, we have determined, the HOMO energy levels of our donors CPP and TMP by standard extended Hückel calculations.[20]

The HOMO energies obtained in this way are significantly different for the two strained molecules: the HOMO of CPP is found to be 0.305 eV higher in energy than that of TMP.

Strain-mediated modifications of chemical and physical properties or organic molecules are common. In this area, for example, changes in the redox potentials as a function of ring strain have been observed for a series of strained 1,4-naphthoquinones and substituted naphthalenes,[33,34] and these redox potential changes have been reasonably correlated with the HOMO–LUMO energy levels, as determined by EHC.

In the present case, the calculated HOMO energies also account for the rather large difference in oxidation potentials (180 mV) measured for CPP and TMP (Table I), though this correlation is correct only on a purely qualitative basis.[35] More elaborated methods than EHC are needed[36] to obtain more accurate correlations.

(d) ^{13}C CPMAS NMR. The solid-state ^{13}C NMR spectra of the unoxidized donors CPP and TMP were first investigated. Both spectra (Figure 5a,b) show a group of resonance lines in the aromatic region (120–160 ppm) and a single line around 26–28 ppm.

The usual gated decoupling pulse technique[16] was employed to differentiate carbon sites that are covalently bonded (protiated) or structurally close to hydrogen atoms from other carbon posi-

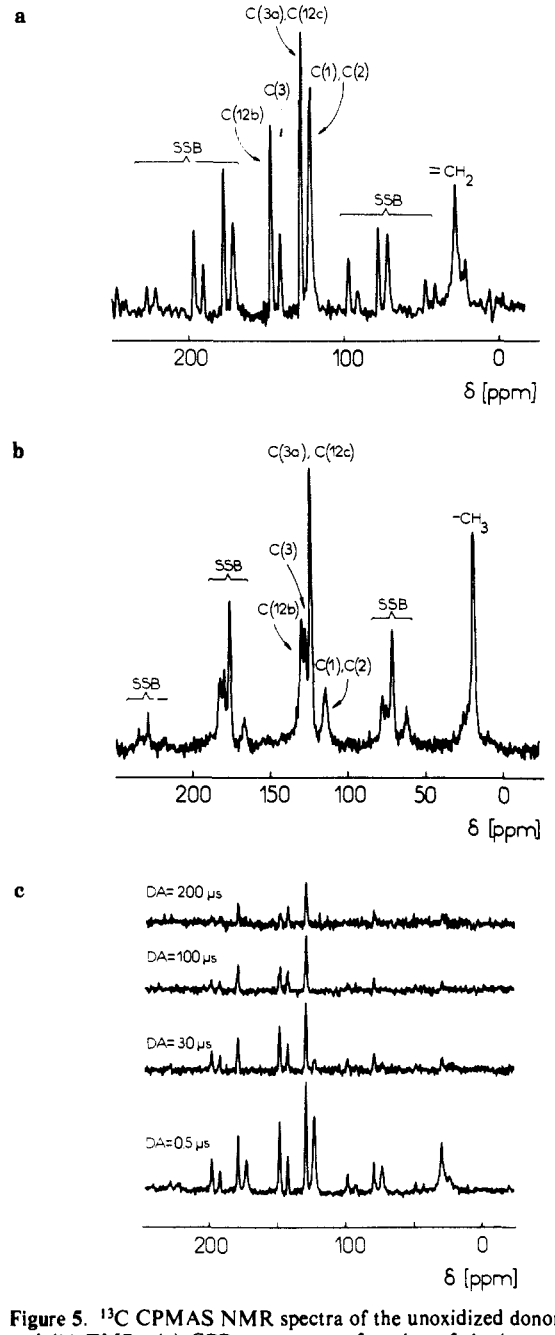

Figure 5. ^{13}C CPMAS NMR spectra of the unoxidized donors (a) CPP and (b) TMP. (c) CPP spectra as a function of the increasing gated decoupling delays (DA) from 0.5 to 200 μs; SSB stands for side spinning bands.

tions. Thus, even a small delay of gated decoupling, 10 μs, considerably reduces the intensities of the resonance lines at 28

(33) Ricke, R. D.; Rich, W. E.; Ridgway, T. H. *J. Am. Chem. Soc.* **1971**, *93*, 1962.

(34) Ricke, R. D.; Bales, S. E.; Meares, C. F.; Rieke, L. I.; Milliren, C. M. *J. Org. Chem.* **1974**, *39*, 2276.

(35) Another qualitative correlation is found by comparing the calculated HOMO–LUMO gaps and the UV–vis spectra. Considering the longest wavelength transitions (Clar's p bands), the sign of the wavelength shift corresponds to these gaps's modification, found to be 0.54 eV wider for **2**. The order of magnitude of the measured shift (~2 nm) of this band is however far from the calculated gap difference (interesting modifications are also observed for the two spectra, when the extinction coefficients are considered).

(36) Reinolds, C. A.; King, P. M.; Richards, W. G. *J. Chem. Soc., Chem. Commun.* **1988**, 1434. See also: Fry, A. J.; Fox, P. C. *Tetrahedron* **1986**, *42*, 5266.

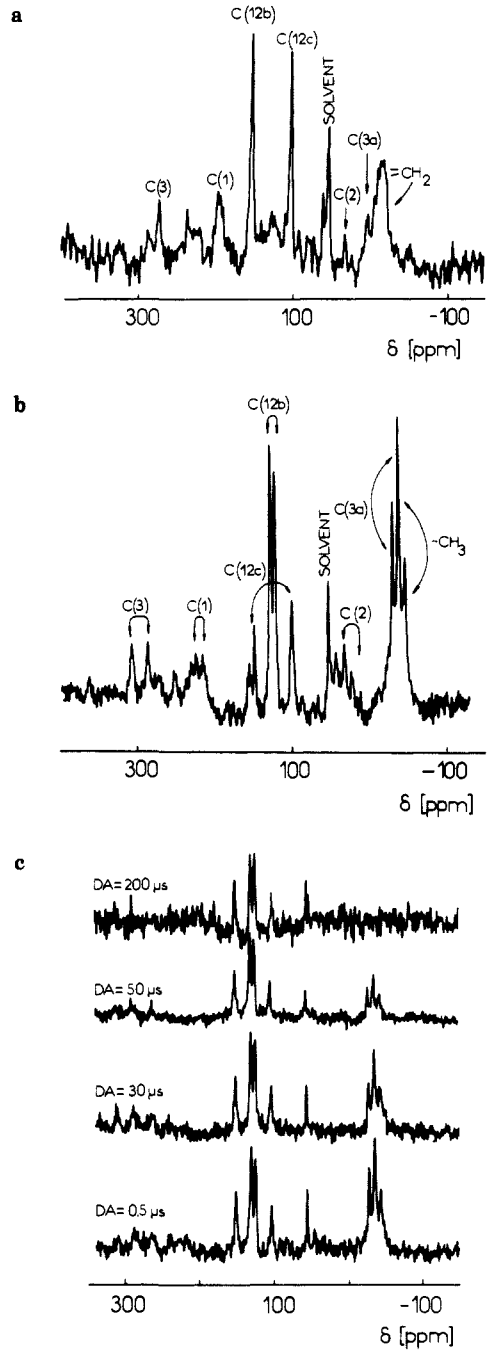

Figure 6. ^{13}C CPMAS NMR spectra of the radical-cations salts (a) $CPP_2PF_6{\cdot}CH_2Cl_2$ and (b) $TMP_2PF_6{\cdot}CH_2Cl_2$. For the assignments, see the text. (c) The $TMP_2PF_6{\cdot}CH_2Cl_2$ spectra as a function of the gated decoupling delays (0.5–200 μs).

and 121 ppm for CPP (Figure 5a,c); the first line is attributed to the methylene bridge carbons and the second one to the protiated carbons C(1) and C(2). The same procedure applied to TMP allows one to distinguish, without ambiguity, the resonance lines at 26 (methyl group) and 121 ppm [C(1) and C(2) carbons]. Then, considering the proximity of the methylene bridge (or CH_3), the lines at 140 (CPP) and 135 ppm (TMP) are assigned to C(3).

The identification of other carbon atoms is experimentally more difficult, the other resonance lines being almost unaffected by longer times (200 μs) of gated decoupling. Considering the intensities of various lines, the resonances at 127 ppm for CPP (**1**) [131 ppm for TMP (**2**)] are assigned to C(3a) and C(12c). The last resonance is consequently attributed to C(12b) (Table III).

Turning to the spectra of the radical-cation salts prepared from these two donors, dramatic modifications are now observed (Figure 6). The position of all the resonance lines, as compared to the neutral donors, are largely shifted (over ~300 ppm), due to both high-field and low-field shifts; well-resolved signals (14) are found for $TMP_2PF_6{\cdot}CH_2Cl_2$ (Figure 6a), whereas only 7 lines are found for $CPP_2PF_6{\cdot}CH_2Cl_2$ (Figure 6b). By use of the same gated decoupling technique, two groups of lines (or doublets for the TMP salt) are identified: (i) The first group concerns the protiated carbons (or the carbons located in the proximity of protons within the stacks). This group contains the lines that vanish when the decoupling delays are increased; for even very small delays [such as 30 μs, as illustrated for $TMP_2PF_6{\cdot}CH_2Cl_2$ (Figure 6c)] the doublets at 25, 35 and 217, 226 ppm disappear (the corresponding lines for the CPP salt are found at 29 and 195 ppm). These lines are assigned to carbons C(1) and C(2) bonded to hydrogen.

When the delay reaches 50 μs, a considerable decrease of the intensity of the doublets at −36, −44 and −28, −36 ppm for the TMP salt is observed (Figure 6c; DA = 50 and 200 μs); the same phenomenon is also observed at −3 and −18 ppm for CPP salt. We assign these lines respectively to the methyl (methylene for the CPP salt) group and to the C(3a) carbon sites, which are found in the proximity of the former within the donors stacks (see Figure 2). (ii) The second group concerns the lines that are practically not affected by the longest delays; this group includes the remaining quaternary carbons C(3), C(12b), and C(12c). These two NMR shift groups are summarized, for both salts, in the Table IV.

Table IV. Line Positions[a] and the Two-Set Line Assignments Obtained by the Gated Decoupling Technique for $(CPP)_2PF_6{\cdot}CH_2Cl_2$ and $(TMP)_2PF_6{\cdot}CH_2Cl_2$

	line positions[d]	
carbon sites	$(CPP)_2PF_6{\cdot}CH_2Cl_2$	$(TMP)_2PF_6{\cdot}CH_2Cl_2$
C(1), C(2)[b]	195	216, 226 (221)
	29	34, 25 (30)
C(3a) $-CH_2-$,	−18	−44, −36 (−40)
(or CH_3)	−3	−36, −28 (−32)
C(3), C(12c),	274	310, 288 (298)
C(12b)[c]	154	150, 102 (126)
	102	129, 124 (127)

[a] In ppm from Me_4Si. [b] Lines that are affected by gated decouplings. [c] Lines not affected by gated decoupling. [d] Mean values (parentheses) are used for the graphical assignments based on the spin density maps, for discussion of the multiplicities, see the text.

At this stage, more precise assignment of the resonance lines to individual carbons within each group is difficult; before a more detailed analysis of the spectra is possible, the large dispersion of the spectral lines of the conducting salts must be addressed. These displacements, as compared to the unoxidized solids, are known as the Knight shifts and they arise from the interactions of the conduction electron gas with the ^{13}C nuclei; the assignments of all lines, that is, the quantitative knowledge of the Knight shifts, needs first a more detailed insight into this phenomenon.

Knight Shifts and the Electron Spin Distributions. The hyperfine interaction between conduction electron spins and nuclear spins, in metals, results in frequency shifts of the nucleus i, the Knight shifts (K_i). K_i is expressed by eq 1, where γ_e and γ_n are, respectively, the gyromagnetic ratios of the electron and the nucleus; χ_p is the Pauli spin susceptibility, and A_i is the isotropic part of the electron–nuclear hyperfine coupling constant.

$$K_i = \frac{\Delta H_i}{H} = \frac{A_i \chi_p}{h \gamma_e \gamma_n} \quad (1)$$

In organic (1-D) metals the electron conduction involves π-orbitals, and the hyperfine constant A_i, calculated for π electron radicals,[37] has the form

$$A_i = a_i \rho_i^{\pi} + \sum_K a_{ij} \rho_i^{\pi} \quad (2)$$

Here a_i and a_{ij} are the $(\sigma - \pi)$ interaction parameters, and ρ_i^{π} and ρ_j^{π} the π spin densities on the considered site i and on the closest surrounding sites j of the π electron carbon frame. The

(37) Karplus, M.; Fraenkel, G. K. *J. Chem. Phys.* **1961**, *35*, 1312.

Table V. Calculated Spin Densities and the Derived Hyperfine Coupling Constants A_i of Unsubstituted Perylene, CPP, and TMP

carbon	spin densities $[A_i]$[a]			
	perylene[b]	perylene[c]	CPP	TMP
C(1)	+0.152	+0.059	+0.1207 [+13.31]	+0.1461 [+14.76]
C(2)	−0.068	−0.011	−0.0422 [−17.01]	−0.0319 [−14.88]
C(3)	+0.205	+0.079	+0.2083 [+22.02]	+0.1546 [+17.43]
C(3a)	−0.080	−0.017	−0.0741 [−21.06]	−0.0808 [−20.35]
C(12c)	−0.033	−0.005	−0.0380 [−0.91]	−0.0364 [−1.84]
C(12b)	+0.013	+0.022	+0.0073 [−2.89]	+0.0243 [−3.16]
substituent (methyl or methylene)			+0.0055 [−8.54]	+0.0027 [−6.28]

[a] In MHz; calculated from eq 2 with the $(\sigma - \pi)$ interaction parameters: a_i = +99 MHz (C_iHC_2 fragment) or +85 MHz (C_iC_3 fragment) a_{ij} = −39 MHz.[37] For the substituents the calculations include the small spin density contribution from the out-of-plane H atoms (see Experimental Section for the numerical values). [b] Present work. [c] Reference 17e.

knowledge of the unpaired spin density distributions is therefore a valuable means to calculate K_j (as long as the value of χ_p is available) and is needed to assign precisely the spectral lines.

We have calculated the π spin densities $\rho_{i,j}^{\pi}$ in the present perylene series. A first-order perturbative configuration interaction (CI) derived from the method of Hoijtink[21] was employed. In this approach, the electronic wave function ψ is approximated as

$$\psi = \psi_0 + \psi_1$$

ψ_0 is the zeroth-order approximation obtained with the MOs from the EHC;[20] and ψ_1 is the first-order perturbative correction:

$$\psi_1 = \sum_{k \neq 0} \Phi_K \langle \Phi_K | V | \psi_0 \rangle / (E_0 - E_K)$$

The difference between the exact Hamiltonian H and the zeroth-order Hamiltonian H_0 defines here the perturbation Hamiltonian V.

Within this approximation[21] the π spin density ρ_i^{π} on atom i is

$$\rho_i^{\pi} = 2 \sum_{K \neq 0} \langle \psi_0 | 2S_z D_i | \Phi_K \rangle \langle \Phi_K | V | \psi_0 \rangle / (E_0 - E_K)$$

Here, S_z is the electronic spin operator and D_i is defined by the matrix elements of eq 3, where φ_p and φ_q are the π molecular

$$\langle \varphi_p | D_i | \varphi_q \rangle = C_{ip} C_{iq} \qquad (3)$$

orbitals (from EHC) and C_{ip} and C_{iq} the coefficients of the corresponding LCAO expansion; Φ_k is the zeroth order wave function of an excited state obtained by substitutions of one or several virtual orbitals for the same number of occupied ones in ψ_0.

The calculated spin densities ρ^{π} (see Experimental Section for the details of the calculations) for CPP and TMP and the corresponding derived hyperfine constants A_i are summarized in Table V; the values for perylene itself, as well as the values available in the literature for the latter,[17e] which had been calculated by the McLachlan perturbation method,[38] are also included.

It should be noted that the presently calculated spin densities are obtained after rather drastic approximations (zeroth-order wave functions of radical cations obtained from MOs of the neutral molecules, zero differential overlap approximation in the evaluation of the perturbative operator and the use of the perturbative CI only at first order, and use of standard parameters without specific optimizations, in particular a_i and a_{ij}) so the accuracy of these values, for which no "direct" experimental determination is possible, has to be carefully examined. A comparison of our π spin densities, calculated for perylene, with those of the literature[17e] (Table V) shows similarities (signs and magnitudes) exist for both groups: in fact, a linear correlation between these two sets of numerical values (with an average deviation of $\sim 5 \times 10^{-3}$) is found; however, the significant differences for the individual spin densities point out the limits of both types of empirical calculation methods. Therefore, the ρ_i^{π} (and A_i) values, obtained for CPP- and TMP-based materials have to be considered more precisely as a general pattern (vide infra) than an accurate numerical determination of the spin density of every single carbon atom.

(38) McLachlan, A. D. *Mol. Phys.* **1960**, *3*, 233.

Table VI. Line Assignments of the $(CPP)_2PF_6 \cdot CH_2Cl_2$ Salt Based on Spin Density Maps

carbon[a]	Knight shifts before graphical assignts[b]	assigned Knight shifts[c] (line positions)	calcd Knight shifts[d]
→ C(1)	74, −92	74 (195)	78
→ C(2)	74, −92	−92 (29)	−100
C(3)	−38, 14, 134	134 (274)	129
→ C(3a)	−130, −145	−130 (−3)	−123
C(12c)	−25, 27, 147	−25 (102)	−5
C(12b)	−44, 8, 128	8 (154)	−17
→ $-(CH_2)_2-$	−31, −46	−46 (−18)	−50

[a] Lines affected by gated decouplings (arrow), as distinguished from the unaffected subgroup; Knight shifts in ppm from Me_4Si. [b] These values (before the graphical assignments) are obtained by subtracting the assigned chemical shifts of the neutral donor (Table III) from the values (after all possible permutations) of the measured nonassigned shifts of the salt within each particular subgroup of carbons (Table IV). [c] Graphically assigned Knight shift values (see Figure 7). [d] Calculated from eq 1; corresponds to $\chi_p = 1.4 \times 10^{-4}$ emu·mol^{-1}.

Line Assignments. These calculated spin density distributions and the resulting electron–nuclear hyperfine coupling constants A_i are now used to obtain a more precise assignment of various spectral lines for both radical-cation salts, through a simple graphical approach.

Starting with the $(CPP)_2PF_6 \cdot CH_2Cl_2$ salt, let us first consider the resonance lines at 29 and 195 ppm, already assigned unambiguously by gated decoupling to the C(1), C(2) subgroup (Table VI). The corresponding Knight shift values, defined here as the shifts from the resonance positions of C(1) and C(2) in the neutral donor (121 ppm) (Table III), are equal to −92 and 74 ppm. Taking into account the linear relationship between K_i and A_i (eq 1) and the signs of the calculated A_i for C(1) and C(2) (Table V), the Knight shift K_i = 74 ppm (and consequently the line at 195 ppm) is attributed to C(1); the other K_i value, and the line at 29 ppm, is therefore assigned to C(2). From eq 1, the value of the Pauli susceptibility may now be estimated: $\chi_p = 1.4 \times 10^{-4}$ emu·mol^{-1}; this value is then used to calculate K_i for other carbons (Table VI), and the straight line obtained on a plot of these values vs A_i (Figure 7a) ultimately allows us to assign completely and unambiguously the Knight shifts to the yet unidentified carbons, through a best fit with experimental K_i. The same approach with the TMP salt (taking arbitrarily the center of gravity of the doublets as an estimation of the Knight shifts) leads to a higher estimated value of the Pauli susceptibility, $\chi_p = 2.04 \times 10^{-4}$ emu·mol^{-1},[39] and allows calculation of K_i values (Table VII) as well as the plot of the K_i vs A_i line (Figure 7b).

A satisfying correlation between the experimental K_i values and the calculated A_i constants is also found, although larger differences between the experimental and calculated Knight shifts, as compared to the CPP salt, are observed. For the TMP salt

(39) The presently estimated χ_p values for TMP and CPP salts can be compared to $\chi_p = 0.92 \times 10^{-4}$ emu·mol^{-1} determined for a parent salt prepared from unsubstituted perylene; see: Moritz, I.; Shaheen, S. A.; Hardebush, U.; Schilling, J. S.; Weger, M.; Bender, K.; Schweitzer, D. *Solid State Commun.* **1983**, *48*, 281.

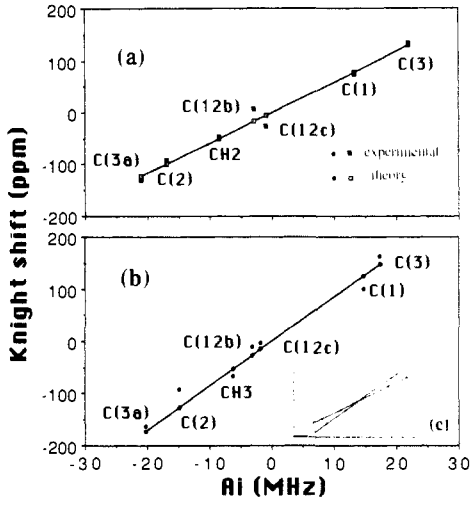

Figure 7. Plots of K_i (Knight shifts in ppm) vs A_i (hyperfine coupling constants in MHZ; Table VII) for (a) $CPP_2PF_6{\cdot}CH_2Cl_2$ and (b) $TMP_2PF_6{\cdot}CH_2Cl_2$. See the text for the graphical procedure and the values of the slopes leading to estimate χ_p values. The inset (c) contains the calculated lines for both solids plotted on the same graph, displaying the slope differences.

Table VII. Line Assignments of the $(TMP)_2PF_6{\cdot}CH_2Cl_2$ Salt Based on Spin Density Maps

carbon[a]	Knight shifts before graphical assignts[b]	assigned Knight shifts (actual line positions)[c]	calcd Knight shifts[d]
→ C(1)	100, -91,	100 (216, 226)	125
→ C(2)	100, -91	-91 (25, 34)	-126
C(3)	-9, -8, 163	163 (288, 310)	148
→ C(3a)	-163, -171	-163 (-36, -28)	-173
C(12c)	-5, -4, 163	-4 (124, 129)	-15
C(12b)	-11, -10, 161	-11 (102, 150)	-27
→ CH_3	-58, -66	-66 (-44, -36)	-53

[a] See footnote *a*, Table VI. [b] The mean values of the various doublets are used to assign the lines. [c] Graphically assigned doublets' mean values (see Figure 7). The graphical differentiation of the doublets C(3a) vs CH_3 and C(12b) vs C(12c) is difficult because of the very small differences of the considered mean values; these two assignments are therefore tentative. [d] Calculated from eq 1; corresponds to $\chi_p = 2.04 \times 10^{-4}$ emu·mol^{-1}, based on the mean values of the doublets.

(Figure 7b), the unambiguous complete assignment of all the lines [C(3a) vs $-(CH_2)-$ and C(12b) vs C(12c)] is, this time, difficult (see footnote c, Table VII) due to the approximation related to the doublets.

Discussion

The strain-induced distorsions of the perylene skeleton, expressed on the molecular level by significant modifications of the redox properties (Table I), do not prevent the preparation of structurally indistinguishable solid radical-cation salts from both CPP and TMP; this similarity is found if the stacking and carbon overlap patterns of the organic building blocks are only considered. These solids are therefore quite adequate to investigate (as we aimed to) the effects of the modifications of the local electronic structures on the bulk conduction properties.

Thus, with ^{13}C CPMAS NMR as a probe of individual sites in organic conducting solids, and considering the locally resolved shifts arising from the presence of the conduction electrons, significant spectral differences are found for the CPP and the TMP salts.

But, an unexpected aspect, also differentiating these NMR spectra, has to be considered first: the decrease of the number of lines, from 14 for the TMP salt to 7 for $(CPP)_2PF_6{\cdot}CH_2Cl_2$ (Figure 6). The magnetic nonequivalencies, within the simplified (counterions and solvent-stripped) organic stacks, do not account for this phenomenon: in this hypothetical model, only seven lines, corresponding to a C_{2h} site symmetry, should be observed for both salts. However, an accurate refinement of the anions and solvent structures has not yet been possible, due to the disorder of the latter. Only a qualitative insight into structural arrangements of PF_6^- and CH_2Cl_2 is presently available through diffuse-scattering experiments (Figure 3). Thus, the site symmetries of the actual solid salts and consequently the number of magnetic nonequivalencies cannot be presently specified. Additional studies of this disorder are required to allow an accurate structural analysis and a rigorous explanation of these differences.[30] Nevertheless, it is clear that the order of the counterions and solvent, which distinguish $(CPP)_2PF_6{\cdot}CH_2Cl_2$ from the more disordered TMP salt, mediates the modifications of the site symmetries of otherwise isostructural organic salts (Table II) and accounts for the observed number of lines.

Apart from the latter question, the measured shifts, as compared to the unoxidized donors, remarkably correlate with the Knight shifts obtained from the calculated A_i values (eq 1; Tables VI and VII) even though mean values for the doublet positions for $(TMP)_2PF_6{\cdot}CH_2Cl_2$ have been considered. These correlations support a simple graphical approach based on K_i vs A_i plots (Figure 7), leading first to the assignments of the spectra, but interestingly allowing also an estimation of the unknown Pauli susceptibility values χ_p of these conducting salts.[40] It is worth noting here that, alternatively,[17g] the Knight shifts expressed as a function of the known susceptibilities, χ_p, provide A_i values and consequently a map of the conduction electron spin density distributions.[41]

In conclusion, the present results clearly establish that tuning the spin density distributions by skeletal deformations of organic donors embedded in similar conductive stacks involves modification of the Knight shift patterns. This stereochemical control of the structure to properties relationship, presently displayed by a ^{13}C CPMAS NMR study, will probably also be reflected in other physical properties of these materials. Thus, the distorsions of the donors might also involve significant changes in the site to site conduction electron paths throughout these solids or, in other words, involve changes in the π orbital overlaps resulting in modified conduction band and bulk conductivity characteristics. These properties are now under further investigation.[28]

Acknowledgment. P.M., A.M., and P.P. gratefully acknowledge generous financial support of this work from the Thomson-Sintra-ASM Co.; A.M. also gratefully acknowledges generous support by the D.R.E.T. P.P. thanks P. Batail for his help in the crystal structure determinations and D. Jérome for his help in the conductivity measurements.

Supplementary Material Available: Atomic numbering scheme for TMP and CPP and fractional atomic coordinates and bond lengths and angles for $(TMP)_2PF_2{\cdot}CH_2Cl_2$ and $(CPP)_2PF_6{\cdot}CHCl_2$ (5 pages). Ordering information is given on any current masthead page.

(40) Measurements of the χ_p values are in progress.

(41) In a very interesting recent report on a series of conductive phthalocyanine materials,[17g] the alternate use of eq 1 led to a linear plot of experimental K_i values vs the corresponding known paramagnetic susceptibilities χ_p. This approach allowed—the variations of A_i values being assumed to be reasonably negligible for the same skeletal position in this closely related large series of phthalocyanine compounds—A_i constants about the carbon framework of the macrocycles to be mapped out. However, the former assumption should be carefully examined because the present A_i values, derived from the calculated spin density distributions (Table V), are found to be significantly different for the same skeletal position for the present closely related solids (see Figure 7).